Visual Neuroscience

ARTICLE

Open Access

https://doi.org/10.48130/vns-0025-0004

Visual Neuroscience **2025**, 42: e004

Microglial phagocytosis involves hyperoxia-induced vessel regression in the neonatal retina

Zhuojun Xu[1,2], Yuan Ma[1,2], Jizhu Li[1,2], Jiejie Zhuang[1,2], Yaping Liu[1,2], Zhuangling Lin[1,2], Baoyi Liu[1,2], Zhuoting Zhu[3,4], Ziye Chen[1,2], Xiaoyue Wei[1,2], Lan Jiang[1,2], Rebiya Tuxun[1,2], Zitong Chen[1,2], Chinling Tsai[1,2], Jing Zhuang[1,2*] and Tao Li[1,2*]

[1] *State Key Laboratory of Ophthalmology, Zhongshan Ophthalmic Center, Sun Yat-sen University, Guangzhou 510060, China*
[2] *Guangdong Provincial Key Laboratory of Ophthalmology and Visual Science, Guangzhou 510060, China*
[3] *Centre for Eye Research Australia, Royal Victorian Eye and Ear Hospital, East Melbourne, 3002, Australia*
[4] *Department of Surgery (Ophthalmology), The University of Melbourne, Melbourne, 3002, Australia*
* Corresponding author, E-mail: zhuangj@mail.sysu.edu.cn; litao2@mail.sysu.edu.cn

Abstract

Oxygen concentration fluctuations are fundamental contributors to retinopathy of prematurity and other retinal neovascular diseases. However, the mechanism of retinal vascular regression under high oxygen stimulation remains unclear. In this study, we employed an oxygen-induced retinopathy mouse model to investigate the role of microglia in hyperoxia-induced vessel regression. Retinal vascular regression characteristics, microglial morphology, and localization were observed using immunofluorescence staining. Expression levels of phagocytic-related factors were analyzed via qPCR and Western blot techniques. Additionally, microglia were partially depleted to verify their functional contributions. TUNEL assay and RNA sequencing were performed to further explore the underlying mechanisms. Our findings indicated that central retinal vascular regression occurs rapidly at an early stage, accompanied by microglial migration and activation. Endothelial cell fragments were detected within microglia, confirming their involvement with phagocytic function, the upregulation of phagocytic-related factors further proved it. Notably, partial depletion of microglia significantly inhibited early retinal vascular regression and reduced endothelial cell apoptosis. Moreover, RNA sequencing and bioinformatics analysis revealed that microglial phagocytosis is regulated by the complement pathway. In conclusion, our study confirms the active participation of microglia in hyperoxia-induced retinal vascular regression through phagocytosis, thereby providing potential targets for early intervention in related diseases.

Citation: Xu Z, Ma Y, Li J, Zhuang J, Liu Y, et al. 2025. Microglial phagocytosis involves hyperoxia-induced vessel regression in the neonatal retina. *Visual Neuroscience* 42: e004 https://doi.org/10.48130/vns-0025-0004

Introduction

Hyperbaric oxygen therapy is essential for newborns with low birth weight to support their lung development. However, it may lead to retinopathy of prematurity (ROP), resulting in ischemia-driven retinal neovascularization and even permanent vision loss[1–4]. Conventional treatments, such as laser therapy[5–7], anti-vascular endothelial growth factor (VEGF) therapy[8–11], and vitreous surgery[12–14], typically intervene in the later stages of the disease, when neovascularization has already formed. Therefore, elucidating the impact of early elevated oxygen concentration on retinal vasculature may offer novel insights into the early diagnosis and treatment of ROP, and significantly enhance our understanding of the pathogenesis of neovascular eye diseases.

The oxygen-induced retinopathy (OIR) mouse model mimics the pathological process of ROP, and it also serves as a valuable tool for investigating the pathogenesis of retinal neovascularization in conditions such as retinal vein occlusion and proliferative diabetic retinopathy. In this model, mouse pups and their nursing dam are exposed to a high-oxygen environment for a specified period, followed by a return to normal air, which sequentially leads to delayed angiogenesis, regression of established superficial retinal vessels, and ischemia-driven retinal neovascularization[15–17]. Currently, most studies focus on the later stages of abnormal neovascularization[18–21], while the earlier process of superficial vascular regression remains poorly understood. Previous studies have attributed hyperoxia-induced vascular regression to oxidative stress-induced damage and endothelial cell apoptosis[22–28]. Besides, the expression levels of several angiogenic cytokines, including VEGF-A and pigment epithelium-derived factor (PEDF), are also involved in this process and are significantly correlated with the extent of avascular zones induced by high oxygen[22,29–32]. However, the precise mechanisms underlying this pathophysiological process have yet to be fully elucidated. Recently, the concept of the neurovascular unit has been introduced, highlighting the importance of cell-to-cell interactions[33–35]. This implies that the relationship between blood vessels and the surrounding cells could be a novel and pivotal focus for exploring the mechanisms underlying retinal neovascular diseases.

Microglia, the resident immune cells of the retina, originate from the yolk sac progenitor cells. In addition to their roles in retinal neuron development, synaptic pruning, and immune surveillance of the extracellular environment, microglia are intimately involved in the formation and maintenance of retinal vasculature[36–38]. During early retinal vascular development, microglia migrate to the neuroretina, where they promote endothelial cell proliferation and migration, and contribute to the branching and anastomosis of the vascular network[39,40]. Moreover, microglia are also implicated in pathological retinal vascularization. It is well-established that microglia become highly activated, transitioning from a resting 'ramified' state to an activated 'amoeboid' state, and become enriched around pathological retinal neovessels by postnatal day 17 (P17) in the OIR model[41]. Numerous studies have further demonstrated that microglia may be regulated through multiple pathways, thereby engaging in and facilitating pathological angiogenesis in the OIR model via mechanisms such as metabolic alterations, exosome secretion, and necrotic apoptosis[42–47]. However, it remains unclear whether microglia are involved in the early retinal

vascular regression process in the OIR model and how they are involved.

PLX5622 is a highly selective, blood-brain barrier-permeable small molecule inhibitor that specifically targets CSF1R, a factor crucial for microglial survival, differentiation, and proliferation. PLX5622 enables the rapid and specific pharmacological depletion of microglia and has been widely used in recent years to treat central nervous system diseases targeting microglia and in mechanistic studies[48,49]. Oral administration of PLX5622 could increase neural circuit connectivity and activity in the adult mouse cortex[50] and improve postoperative cognitive decline in rodents by reducing hippocampal inflammatory mediators and abrogating recruitment of CCR2+ leukocytes[51]. Additionally, PLX5622 efficiently alleviated neural and vascular damage in the retinas of diabetic mouse models[52]. When administered during the proliferation phase in the OIR mouse model, PLX5622 reduces pathological neovascularization at P17[53]. However, its effects on early retinal vascular regression in the OIR model have yet to be explored.

In this study, we employed the OIR mouse model to elucidate the spatiotemporal characteristics of early retinal vascular regression under high oxygen conditions. Concurrently, we revealed the migration and activation of microglia during this pathological process. Partial depletion of microglia using PLX5622 inhibited the process of retinal vascular regression. Furthermore, we employed RNA sequencing, bioinformatics analysis, and molecular biology experiments to explore the underlying molecular mechanisms. These findings shed light on the role of microglia in high oxygen-induced retinal vascular regression, providing novel insights for the diagnosis and treatment of related diseases.

Materials and methods

Animals and ethics statement

Adult (male and female) and newborn C57BL/6J mice were obtained from the Ophthalmic Animal Laboratory, Zhongshan Ophthalmic Center, Sun Yat-sen University (Guangzhou, China). All the animal experiments were approved by the Institution Animal Care and Use Committee of Zhongshan Ophthalmic Center (Permit No.: SYXK (YUE) 2018-0189) and were conducted in accordance with the Association for Research in Vision and Ophthalmology Statement for the Use of Animals in Ophthalmic and Vision Research. Mice were kept on a 12-h light/dark cycle under controlled temperature and humidity conditions.

OIR mouse model

To establish a reliable OIR mouse model, 7-day-old C57BL/6J mouse pups and their lactating mothers were kept in a chamber with an oxygen concentration of 75% ± 2% for five days before being transferred to normoxia (OIR group). Extra nursing dams were prepared in case of fatal pulmonary edema. Body weights were monitored, and the overweight or underweight pups were excluded to minimize the influence of metabolic health. Age-matched pups kept in normoxia served as normal controls (NOX group). Both groups of mice were sacrificed at designated time points, and their eyeballs were extracted for further experimentation.

PLX5622 treatment

To deplete microglia in the retinas of the mouse model, PLX5622 (MCE, Monmouth Junction, NJ, USA) was administered to neonatal mice at a dose of 50 mg/kg daily via intraperitoneal injection, from P4 to P7. The dissolution and dilution of PLX5622 were performed following the manufacturer's instructions. Pups injected intraperitoneally with the vehicle, consisting of DMSO (Sigma Aldrich), ethoxylated hydrogenated castor oil (MCE), and saline at the same time points, served as vehicle controls.

Immunofluorescence

The eyes were enucleated and fixed in 4% paraformaldehyde, followed by the removal of the cornea and lens. For retinal flat mounts, the retinal pigment epithelium and sclera tissue were carefully dissected away, and the cup-shaped retinal tissues were radially cut into four-leaf clover shapes. For retinal cryosections, the cup-shaped ocular tissue was embedded in optimal cutting temperature (OCT) compound and sectioned into 10 μm thick slices. Both whole mounts and cryosections were blocked in a solution containing Triton X-100 (Sigma Aldrich) and 5% BSA (Biofroxx, Einhausen, Germany), followed by sequential incubation with primary antibodies (1:400), secondary antibodies (1:1000), and staining with DAPI (1 μg/mL; Sigma-Aldrich). Finally, an antifade mounting medium was applied for slide mounting. All antibodies used in this study are listed in Supplementary Table S1. Panoramic images of both retinal whole mounts and sections were acquired using the TissueFAXS Q+ system (TissueGnostics, Vienna, Austria), while detailed observations were performed with a confocal microscope (Zeiss, Oberkochen, Germany).

The area of avascular zones in the flat-mounted retina was identified and quantified using Fiji (National Institutes of Health, Bethesda, MD, USA)[54]. The length and area of vessels were measured with AngioTool (University of Warwick, UK)[55]. Four 40X fields of view corresponding to avascular zones were selected in each retina for the morphological analysis of microglia. The axon statistics of microglia, a robust indicator of activation level, were also carried out by the skeleton plug-in in Fiji, which was consistent with a previous study[38].

The number of microglia in retinal sections was quantified to determine their longitudinal migration pattern under high oxygen stimulation. Retinal sections through the optic nerve were evenly divided into three regions based on their distance from the optic nerve: the central zone (C), the mid-peripheral zone (MP), and the peripheral zone (P). Vertically, the sections were stratified according to retinal anatomical layers: the nerve fiber and ganglion cell layer (NFL + GCL), the inner plexiform layer (IPL), the inner nuclear layer (INL), the outer plexiform layer (OPL), and the outer nuclear layer (ONL). The microglia count in each zone was recorded, and the results were summarized.

Terminal Deoxynucleotidyl Transferase dUTP Nick End Labeling (TUNEL) assay and CD31 staining

Retinal cryosections were subjected to Terminal Deoxynucleotidyl Transferase dUTP Nick End Labeling (TUNEL) assay, followed by CD31 staining. TUNEL assay (Elabscience, Wuhan, China) was performed following the manufacturer's protocols. CD31 immunofluorescent staining was carried out using previously described methods. Nuclei were counterstained with DAPI for 10 min. Images were acquired using a confocal microscope.

Western blotting

OIR and NOX mice were sacrificed after 16 h of high-oxygen stimulation, and retinas were harvested for protein extraction using RIPA buffer (Beyotime, Shanghai, China) supplemented with PMSF (Beyotime). Protein concentrations were determined using a BCA assay kit (Beyotime). The protein samples were then subjected to electrophoresis and transferred onto polyvinylidene fluoride (PVDF) membranes. The membranes were blocked and incubated with the appropriate primary antibody (1:1000) overnight at 4 °C, followed by incubation with the corresponding horseradish peroxidase (HRP)-conjugated secondary antibody (1:10000) at room temperature for

2 h. Protein bands were visualized using ECL high-sensitivity chemiluminescence reagent (Millipore, Burlington, MA, USA), and their intensities were quantified using Fiji software. The antibodies utilized in this experiment are detailed in Supplementary Table S1.

Quantitative real-time PCR

Retinal tissue collection from OIR and NOX mice was performed after 16 h of high-oxygen stimulation, following the protocol described above. Total RNA was extracted from the retinas using a Trizol reagent kit (Invitrogen, Carlsbad, CA, USA) according to the manufacturer's instructions. Approximately 500 ng of RNA was used for reverse transcription with HiScript Q RT SuperMix (Vazyme, Nanjing, China). Quantitative real-time PCR was performed to measure the expression level of target genes using ChamQ SYBR Color qPCR Master Mix (Vazyme, Nanjing, China), with β-actin serving as the internal reference. The primer sequences used in this experiment are listed in Supplementary Table S2.

Transcriptome sequencing and bioinformatics analysis

The two groups of mice (OIR and OIR + PLX5622) were sacrificed, and total RNA was extracted from the retinal tissues using a Trizol reagent kit according to the manufacturer's protocol. After assessing RNA quality, mRNA was enriched and reverse-transcribed to synthesize cDNA. PCR amplification was then performed to construct a gene library after purifying and repairing the double ends of the cDNA. The library construction and sequencing were conducted using Illumina Novaseq6000 (Gene Denovo Biotechnology Co, Guangzhou, China). Differentially expressed genes (DEGs) were identified using the 'DESeq2' package. DEGs with a fold change ≥ 1.5 and p value < 0.05 were chosen for further analysis. Pathway enrichment analysis was performed using the Kyoto Encyclopedia of Genes and Genomes (KEGG) database.

Statistical analysis

All quantitative data were presented as mean ± standard deviation (SD). Intergroup differences between mean values were analyzed using a two-tailed, unpaired Student's t-test for comparisons between two groups and ordinary one-way ANOVA for comparisons involving more than two groups. Statistical significance was set at $p < 0.05$, and is denoted as * $p < 0.05$, ** $p < 0.01$, *** $p < 0.001$, **** $p < 0.0001$. The results reported in this study were derived from three independent experimental replicates. Data analysis and statistical computations were performed using GraphPad Prism v9.4 (GraphPad Software, La Jolla, CA, USA).

Results

Retinal vascular regression after short-term hyperoxic stimulation

The regression of retinal vascular induced by hyperoxic stimulation was the initial pathological process in the OIR model. To investigate the characteristic of the retinal vascular regression, P7 pups were exposed to 75% oxygen for varying durations: 2 h (P7 + 2 h), 6 h (P7 + 6 h), 12 h (P7 + 12 h), 1 d (P8), 3 d (P10), 5 d (P12), and 5 d followed by 1 d of recovery in normal air (P13), respectively. The results revealed that although the high-oxygen stimulus persisted for 5 d, segmental vascular collapse in the central region of the OIR retina occurred at a very early stage. Specifically, the central avascular zone first enlarged after 12 h of excessive oxygen stimulation. The area ratio of the central avascular region to the whole retina had reached 39.87% after 1 d, approximated to its maximum of 41.57%, which was observed after 5 d of hyperoxic stimulus at P12 when the OIR mice were moved out from the oxygen chamber (Fig. 1b). In summary, the retinal vessels regressed after short-term high-oxygen stimulation.

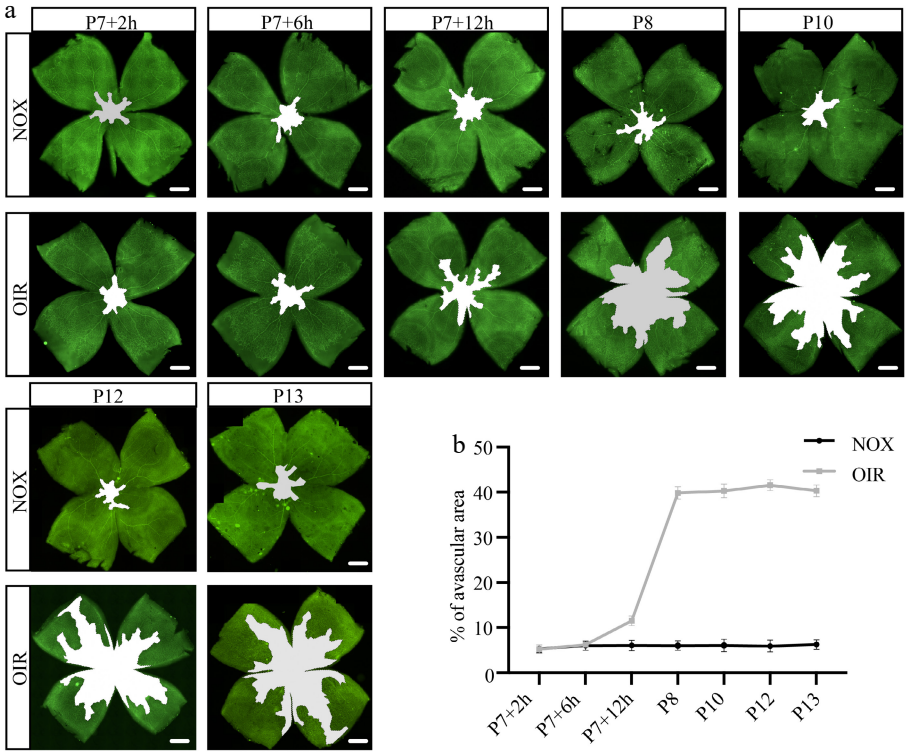

Fig. 1 Characteristics of retinal vascular regression under hyperoxic stimulation. (a) Representative panoramic images of retinal flat mounts stained with CD31 (green) at various time points, the white regions indicate avascular areas. Scale bar: 500 μm. (b) Proportion of avascular area in whole retina at different time points under hyperoxic stimulation. N = 5/group.

Migration and activation of retinal microglia after hyperoxic stimulation

To verify whether microglia are involved in the process of vascular rupture and subsequent clearance of vascular fragments, we performed ionized calcium-binding adapter molecule 1 (Iba1) immunofluorescent staining of retinal cryosections. We selected P7 + 16 h, the time point at which peak retinal vascular regression occurs, to conduct further observations. The retinal cryosections were divided into distinct regions, and the number of Iba1+ microglia was counted separately in each region (Fig. 2a). Our findings proved that although hyperoxia stimulation does not influence the total number of retinal microglia, their distribution has been changed. Interestingly, we found more Iba1+ microglia in NFL + GCL of the central retina under high-oxygen conditions compared to normal air. In contrast, the number of Iba1+ microglia decreased both in INL of the central retina and NFL + GCL of the peripheral retina (Fig. 2b). These results indicated the migration of microglia towards the innermost layer of the central retina, which corresponds spatially and temporally to the breakdown of retinal vessels under high oxygen stimulation.

Since the morphology of microglia can reflect its function and activated state, we observed the morphological characteristic of microglia within retinal flat mount stained with Iba1 at P7 + 16 h (Fig. 2c). Overall, the superficial microglia (mainly located at NFL + GCL) exhibited a relatively activated morphology compared to the deep microglia (corresponding to the deep vascular network located at OPL) under both normoxia and hyperoxia. We analyzed the microglial skeleton in the deep retina using Fiji. The results showed that compared with the NOX group, microglia in the OIR group have fewer branches and endpoints (Fig. 2d, e). It suggested that microglia are relatively activated in a hyperoxic environment. A previous study reported that the 'ball-and-chain' structure of the 'phagocytic cup' is related to the phagocytic phenotype of microglia[56]. Our findings indicated that, compared to the NOX group, hyperoxic stimulation caused more microglia to exhibit the 'ball-chain' phagocytic phenotype in the superficial layer of the retina (Fig. 2f, g). Together, these results suggested that retinal microglia migrate and activate under high-oxygen stimulation.

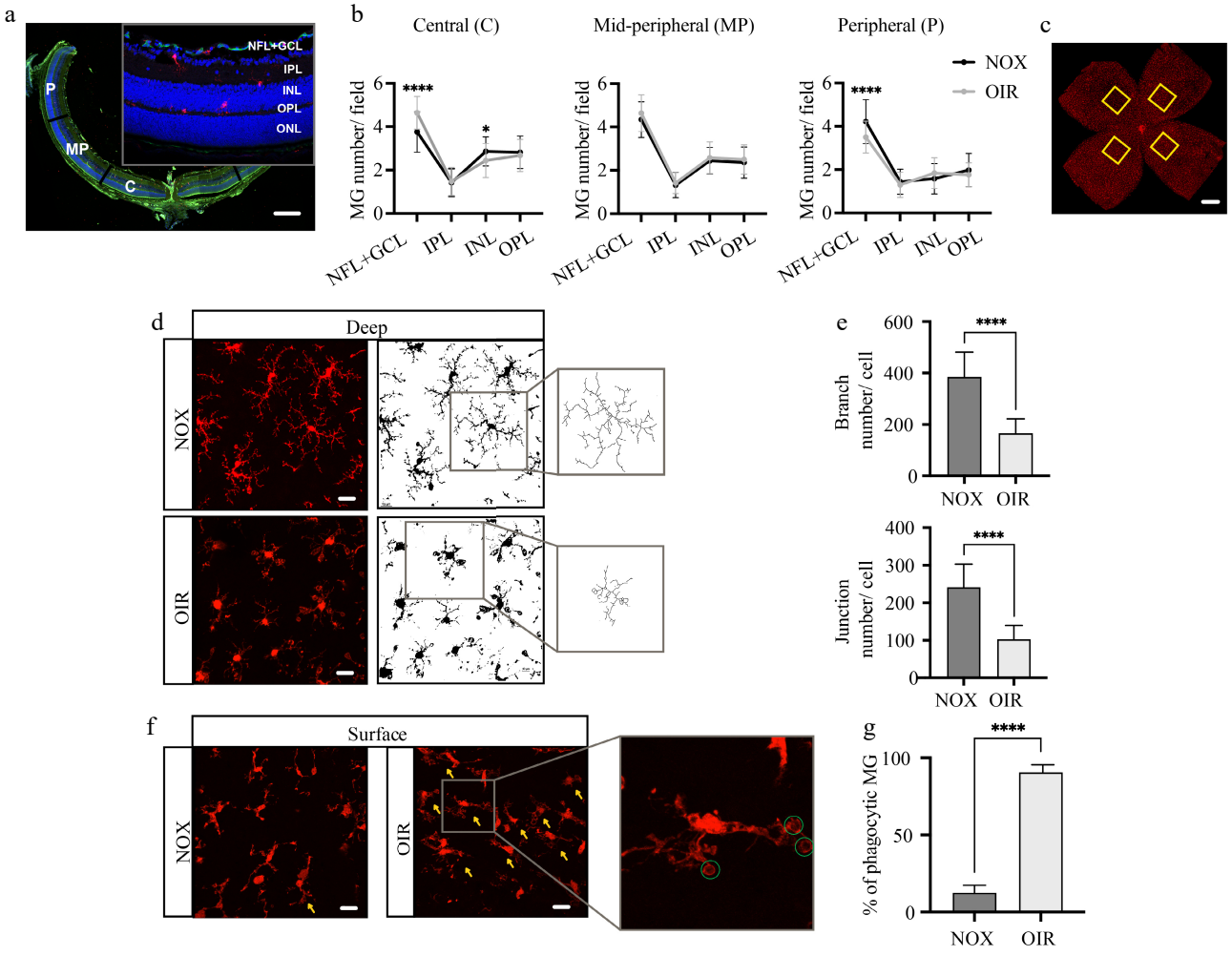

Fig. 2 Migration and activation of retinal microglia following short-term hyperoxic stimulation. (a) Representative image of retinal sections stained with CD31 (green), Iba1 (red), and DAPI (blue), illustrating the retinal regions and layers used for cell counting. Scale bar: 200 μm. (b) Quantification of microglial numbers in different regions at P7 + 16 h. N = 5/group. (c) Representative image of retinal flat mounts stained with Iba1 (red), the yellow boxes indicate areas selected for high-magnification imaging and subsequent cellular morphology analysis. Scale bar: 500 μm. (d) The morphological features of deep Iba1+ (red) microglia at P7 + 16 h, along with representative binary and skeletonized images of the microglia generated using Fiji software. Scale bar: 20 μm. (e) Quantification of the average branch and junction numbers per cell. N = 5/group. (f) The morphological features of superficial Iba1+ (red) microglia at P7 + 16 h, the yellow arrowheads indicate phagocytic morphology with 'ball-and-chain' structures, and the green circles highlight the phagocytic cups. Scale bar: 20 μm. (g) The percentage of phagocytic microglia per field. N = 5/group.

Retinal microglia phagocytize vascular endothelial cells under hyperoxia

Double staining of Iba1 and CD31 was performed at P7 + 16 h to investigate the relationship between microglia and hyperoxia-induced vascular breakdown. Intriguingly, numerous microglia containing CD31+ endothelial cell debris were observed in the OIR retina, while no such phenomenon had been observed in the retina of the NOX group (Fig. 3a, b). This finding provided direct and compelling evidence that microglia are involved in hyperoxia-induced vascular breakdown through phagocytosis.

To explore the phagocytic capacity of retinal microglia, we extracted RNA from the whole retina and conducted quantitative real-time PCR assays for several phagocytosis-associated genes[57,58]. The results showed a significant increase in the mRNA expression of CD68, triggering receptor expressed on myeloid cells 2 (TREM2), and apolipoprotein E (APOE) following hyperoxic stimulation (Fig. 3c). CD68 is a specific marker for activated phagocytic microglia and macrophages. Immunofluorescence staining exhibited that CD68 expression in both the NOX and OIR groups was localized exclusively within Iba1+ microglia in the retina (Supplementary Fig. S1), indicating that CD68 level directly reflects the phagocytic capacity of microglia. We further confirmed that high-oxygen treatment upregulates CD68 expression at the protein level using Western blot analysis (Fig. 3d). In addition, multiple immunofluorescent staining of Iba1, CD31, and CD68 revealed that Iba1+ microglia, which is co-localized with CD31+ endothelial cell fragments, also express high levels of CD68 (Fig. 3e), verifying the phagocytic phenotype of these cells. Our findings thus demonstrated the phagocytic activity of microglia in response to hyperoxia stimulation.

Partial depletion of microglia inhibits early retinal vascular breakdown induced by hyperoxia

We depleted microglia with PLX5622, a highly selective and blood-retinal barrier permeable CSF1R inhibitor, to further elucidate the vital role of microglia. The medication treatments were administered from P4 to P7, the pups with their nursing dams were put into the oxygen chamber after the last injection, and euthanized at different time points for further experiments (Fig. 4a). At P7 + 16 h, over 60% of microglia were efficiently depleted (Fig. 4b, c) without affecting their survival or nutritional status (Supplementary Fig. S2). CD31 immunofluorescence staining of retinal flat mount revealed that the vessels of the PLX5622-treated group remained almost intact whereas the central retinal vessels in the vehicle group experienced segmental collapse after 16 h of hyperoxic stimulation (Fig. 4d). Statistically significant differences were observed between the two groups regarding their respective vessel area, vessel length, and the number of junctions (Fig. 4e). However, with prolonged high-oxygen exposure for 5 d, vascular breakdown in the central retina still occurred in the PLX5622-treated group, but the avascular

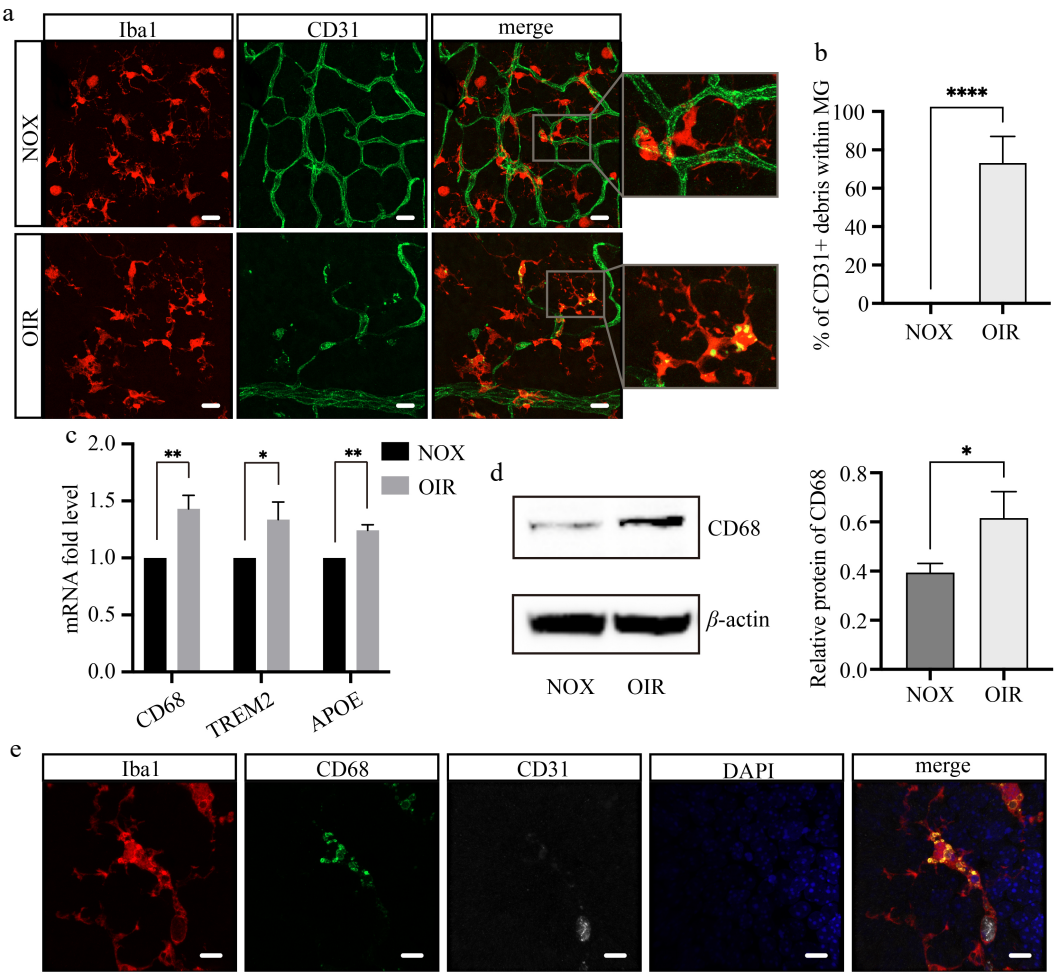

Fig. 3 Retinal microglia phagocytize vascular endothelial cells under hyperoxia. (a) Confocal images of retinal flat mounts stained with Iba1 (red) and CD31 (green) at P7 + 16 h. Scale bar: 20 μm. (b) The proportion of microglia containing CD31+ debris per field. N = 5/group. (c) The mRNA expression levels of genes related to phagocytosis. N = 3/group. (d) The protein expression and relative level of CD68. N = 3/group. (e) Multiple staining of Iba1 (red), CD31 (white), CD68 (green), and DAPI (blue) on the wholemount retina of OIR mice. Scale bar: 10 μm.

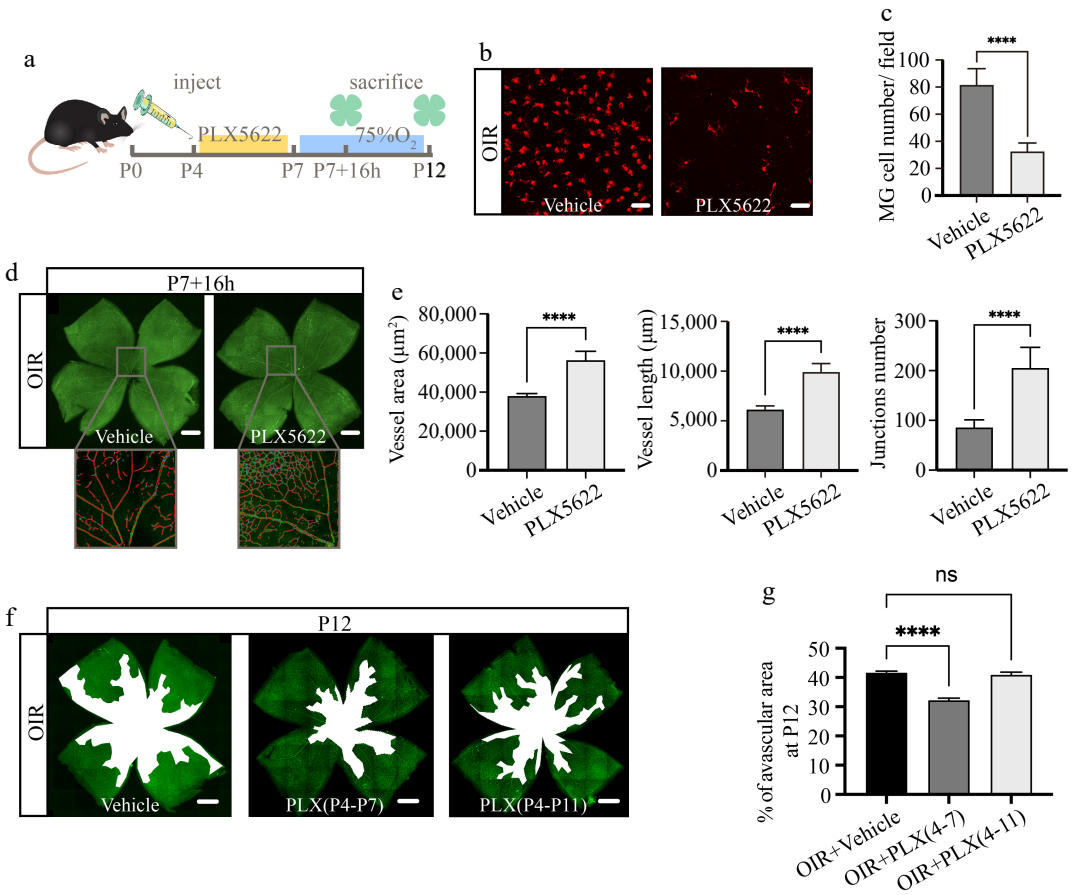

Fig. 4 Partial microglial depletion inhibits early retinal vascular breakdown induced by hyperoxia. (a) Schematic diagram and timeline of microglial depletion and subsequent observation. (b) Immunofluorescence staining of Iba1 (red) on retinal flat mounts at P7 + 16 h. Scale bar: 50 μm. (c) Quantification of Iba1+ microglial numbers per field. N = 5/group. (d) Immunofluorescence staining of CD31(green) on retinal flat mounts, with magnified vascular structure diagrams at P7 + 16 h. Scale bar: 500 μm. (e) Quantification of vessel area, vessel length, and junction numbers per field. N = 5/group. (f) Panoramic images of retinal flat mounts stained with CD31 (green), the white regions indicate avascular areas. Scale bar: 500 μm. (g) Proportion of avascular area in whole retina at P12. N = 5/group.

zone in the central retina was smaller compared to the vehicle group, while continuous administration of PLX5622 from P4 to P11 did not affect the avascular area at P12 compared to the vehicle group (Fig. 4f, g). These results collectively suggested that retinal vascular changes induced by oxygen fluctuations might be regulated by multiple mechanisms, with microglia performing different functions at different stages.

Microglial depletion alleviates endothelial cell apoptosis under high-oxygen conditions

To investigate whether the phagocytic role of microglia initiatively contributes to the breakdown of retinal vessels or passively participates in the clearance of fragmented vascular tissue after breakdown, we conducted apoptosis detection in retinal cryosections of mice with partial microglial depletion at P7 + 16 h. The results revealed that, compared to the normoxic control group, the hyperoxic group exhibited more TUNEL+ apoptotic cells. However, the total number of apoptotic cells was comparable with or without PLX5622 treatment (Fig. 5a, b). Although microglial depletion did not alter the total number of apoptotic cells, TUNEL and CD31 co-staining revealed a significant reduction in the proportion of apoptotic vascular endothelial cells with microglial depletion under hyperoxia conditions (Fig. 5c). It strongly confirmed the initiative involvement of microglia in the process of retinal vascular breakdown.

The complement pathway regulates hyperoxia-induced microglial phagocytosis

Transcriptome sequencing was performed at P7 + 16 h to investigate the mechanisms underlying microglial phagocytosis under hyperoxic conditions. A total of 139 upregulated and 435 downregulated DEGs were identified between the PLX5622 + OIR group and the OIR + Vehicle group (Fig. 6a, b). KEGG pathway enrichment analysis of the 435 downregulated DEGs revealed that five of the top 10 enriched pathways were related to vascular inflammation and angiogenesis (Fig. 6c), indicating that microglial depletion indeed impacts the retinal vasculature in the OIR model. Additionally, the complement pathway was highly enriched among the downregulated DEGs. Representative genes from the complement pathway were selected for quantitative real-time PCR validation, and their expression was further examined in the NOX group. The results confirmed that complement pathway-related genes (C1qa, C1qb, C1qc, C3ar1, C4b) were upregulated under hyperoxic conditions and downregulated following microglial depletion (Fig. 6d). Notably, immunofluorescence triple staining revealed that C3ar1 was detected in phagocytic microglia containing CD31+ endothelial cell debris in the retinal flat mounts of the hyperoxia-treated group, suggesting its critical role as a regulatory factor (Fig. 6e). These findings demonstrated that the complement pathway regulates microglial phagocytosis under hyperoxic conditions.

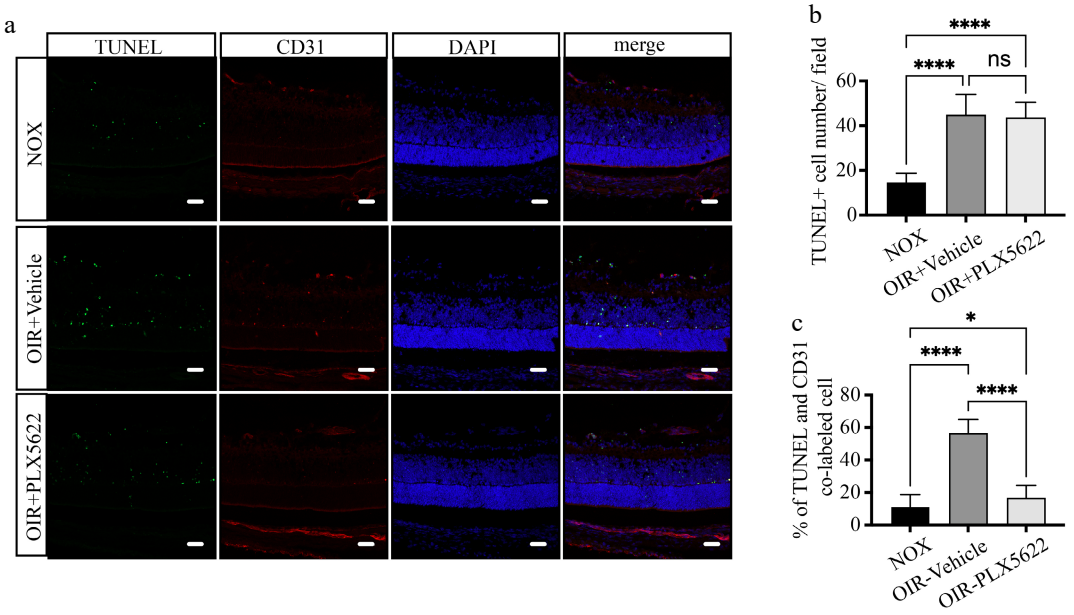

Fig. 5 Microglial depletion alleviates early endothelial cell apoptosis under high-oxygen conditions. (a) Representative images of retinal cryosections stained with TUNEL (green), CD31 (red), and DAPI (blue) at P7 + 16 h. Scale bar: 30 μm. (b) Quantification of TUNEL+ apoptotic cell numbers per field. N = 5/group. (c) The proportion of apoptotic endothelial cells co-labeled with TUNEL and CD31. N = 5/group.

Discussion

Vascular regression is the initial pathological change of the retina under fluctuations in environmental oxygen concentration. Previous studies often considered the early appearance of avascular areas and subsequent neovascularization as two independent events, with a primary focus on the pathological processes and mechanisms of the latter, while paying less attention to the former. CD31, also known as platelet-endothelial cell adhesion molecule, is a member of the immunoglobulin superfamily. Although it is widely expressed on the surface of various cell types, including endothelial cells, platelets, neutrophils, monocytes, and certain types of T cells, it is still commonly used as a constitutive marker for vascular endothelial cells. In this study, CD31 was employed as a marker to achieve clear labeling of retinal blood vessels. In this study, we first observed that although the hyperoxia condition persists for 5 d, both retinal vessel regression and subsequent debris clearance manifest expeditiously, initiating after 12 h of hyperoxia stimulation and concluding within the following 12 h (Fig 1). In-depth research into hyperoxia-induced retinal vascular regression can enhance the overall understanding of neovascular diseases and provide new insights for their treatments.

Microglia, serving as immune surveillance cells resident in the central nervous system and retina, possess phagocytic abilities similar to macrophages and function as custodians for maintaining homeostasis within the organism. The phagocytic activity of microglia represents a double-edged sword. In the central nervous system, for instance, microglia mitigate the progression of neurodegenerative diseases, such as Alzheimer's, by engaging in the phagocytosis of aberrantly accumulated metabolic waste[59,60]. Conversely, excessive phagocytosis of neuronal axons by microglia exacerbates functional impairments within the nervous system[61]. Our observations revealed that microglia exhibit directed migration towards avascular regions, displaying a notably activated cellular morphology and high phagocytic activity, with CD31+ endothelial cell fragments within it (Figs 2 & 3a). These findings indicate that microglia might play a detrimental role in maintaining normal retinal vasculature during the early stages. Targeting microglia for early intervention may offer a new therapeutic strategy for oxygen-induced retinal neovascular diseases, such as ROP.

Numerous studies have reported that microglia become activated in various pathological processes. Pharmacological depletion of microglia has been widely used in mechanistic studies of various diseases and is considered a promising therapeutic strategy. In central nervous system diseases, the depletion of microglia can inhibit the pathological manifestations related to psychosocial stress and behavioral deficits associated with depression[62], alleviate neurodegeneration in Parkinson's disease[63], and delay the onset of autoimmune encephalomyelitis[64]. Additionally, microglial depletion within the eye could effectively mitigate retinal ganglion cell loss following optic nerve injury, and reduce vascular and neuronal damage in the retinas of diabetic mice[65,66] However, microglial depletion is not always beneficial to the organism. In mice with acute infectious encephalomyelitis, microglial depletion exacerbates demyelination severity and impairs myelin regeneration[67]. Similar adverse effects have also been observed in studies related to neonatal hydrocephalus[68]. It highlights the complexity of microglial functions, as they may play markedly different roles in various pathophysiological processes. Furthermore, depleting microglia at different time points within the same disease model can lead to varying outcomes[69,70], underscoring the critical importance of timing in microglia-targeted therapies. In our study, we depleted over 60% of microglia using PLX5622 before entering the oxygen chamber, effectively inhibited early vascular breakdown induced by hyperoxia at P7 + 16 h, and decreased the central avascular area at P12. Additionally, partial depletion of microglia significantly inhibited endothelial cell apoptosis (Figs 4d–g, 5). Our findings demonstrate for the first time that microglia are involved in the regression of normal vasculature before promoting hypoxia-induced retinal neovascularization. Early depletion of microglia before the proliferative phase may represent a novel strategy for early intervention in diseases such as ROP.

Moreover, our study also demonstrated that microglial phagocytosis under hyperoxia conditions may be modulated by the complement pathway. As an integral component of the innate immune system, the complement system can be activated by pathogenic

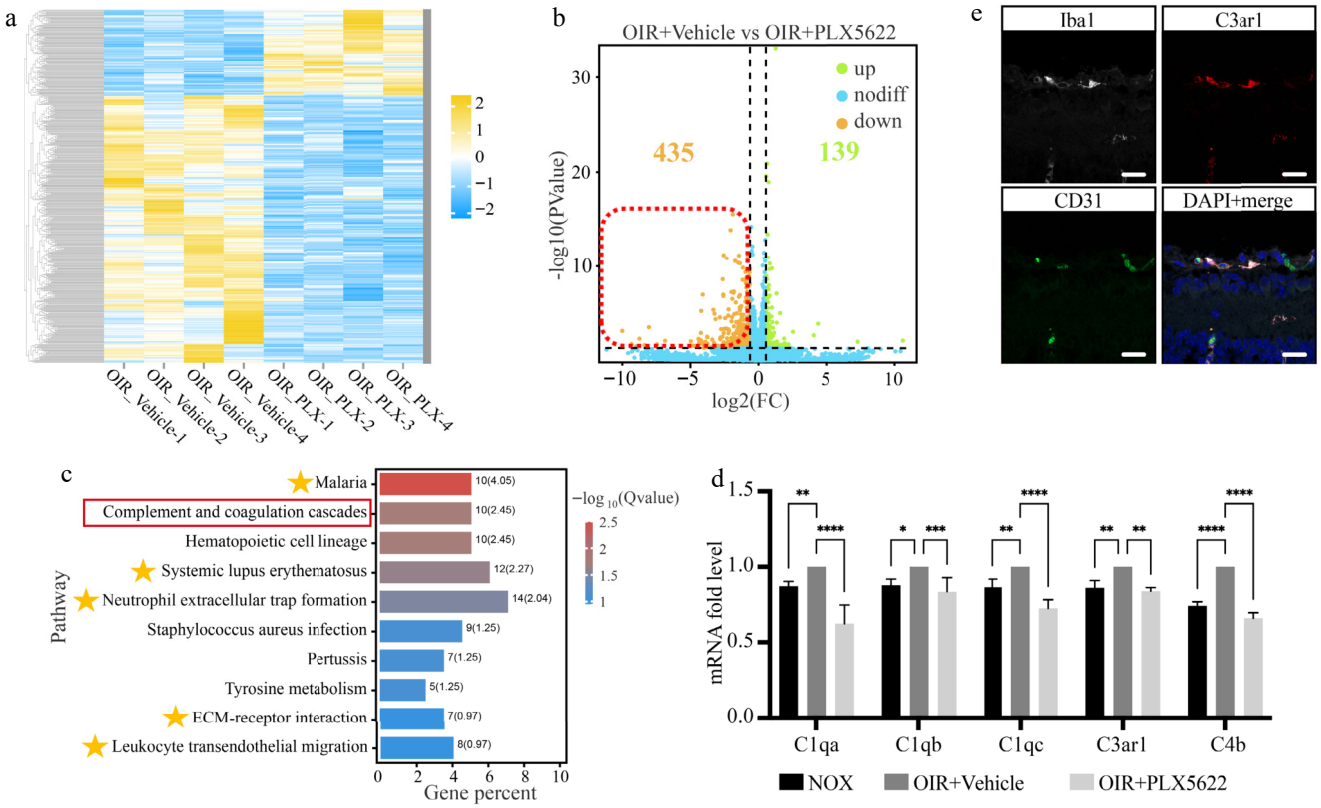

Fig. 6 Hyperoxia-induced microglial phagocytosis is regulated by the complement pathway. (a) - (b) Heatmap and volcano plots of DEG distribution between the OIR + Vehicle and OIR + PLX5622 groups. (c) Top 10 pathways identified by KEGG enrichment analysis of downregulated DEGs. The yellow stars indicate pathways related to vascular inflammation and angiogenesis. (d) The mRNA expression level of the key genes in the complement pathway. N = 3/group. (e) Multiple staining of Iba1 (white), CD31 (green), C3ar1 (red), and DAPI (blue) on the retinal cryosection of OIR + Vehicle mice. Scale bar: 10 μm.

microorganisms, initiating a series of cascade reactions to neutralize toxins, facilitate inflammation, and enhance opsonization, thereby regulating the immunological milieu. The regulation of microglia by the complement pathway and its underlying mechanisms have garnered significant attention from researchers. Within the central nervous system, microglia can mediate age-associated cognitive deficits through complement-dependent synaptic phagocytosis[71]. Besides, excessive synaptic phagocytosis by microglia, which is modulated by the complement signaling pathway, has been implicated in the etiology of depression and Huntington's disease[72,73]. The complement C3a receptor 1 (C3ar1) is a typical G protein-coupled receptor, and microglia with elevated C3ar1 expression have been observed to accumulate around amyloid plaques in murine models of Alzheimer's disease[74]. Similarly, in a mouse model of retinal detachment, heightened C3ar1 expression has been detected within retinal microglia, which is hypothesized to be associated with neuroinflammation and photoreceptor cell apoptosis[75]. Our study confirmed that C3ar1 expression is upregulated under hyperoxia stimulation, and the immunofluorescence staining further verified that its regulatory target is located on microglia (Fig. 6c, d). This suggested that C3ar1 might be the key target in regulating microglial phagocytic activity under hyperoxia conditions.

In conclusion, this study elucidated the mechanism of early retinal vessel regression under high-oxygen stimulation and further highlighted the critical role of microglia in this process. These findings might enhance comprehension regarding the pathogenesis of ROP and other oxygen-induced neovascular diseases, providing novel strategies for its early interventions.

Ethical statements

All the animal experiments were approved by the Institution Animal Care and Use Committee of Zhongshan Ophthalmic Center (Permit No.: SYXK (YUE) 2018-0189) and were conducted in accordance with the Association for Research in Vision and Ophthalmology Statement for the Use of Animals in Ophthalmic and Vision Research as well. The research followed the 'Replacement, Reduction, and Refinement' principles to minimize harm to animals.

Author contributions

The authors confirm contribution to the paper as follows: study conception and design: Xu Z, Ma Y, Zhuang J, Chen Z, Li T, Zhuang J; data collection: Xu Z, Li J, Liu Y, Lin Z, Liu B, Zhu Z, Wei X; analysis and interpretation of results: Xu Z, Jiang L, Tuxun R, Chen Z, Tsai CL; draft manuscript preparation: Xu Z, Zhuang J, Li T. All authors reviewed the results and approved the final version of the manuscript.

Data availability

The datasets generated and analyzed during the current study are not publicly available, but are available from the corresponding author on reasonable request.

Acknowledgments

This work was supported by grants from the National Natural Science Foundation of China (Grant Nos 82271093 and 82070972).

The authors thank the staff of the Public Experimental Platform and Laboratory Animal Center of Zhongshan Ophthalmology Center for assistance in the experiments.

Conflict of interest

The authors declare that they have no conflict of interest. Dr. Zhuoting Zhu is the Editorial Board member of *Visual Neuroscience* who was blinded from reviewing or making decisions on the manuscript. The article was subject to the journal's standard procedures, with peer-review handled independently of this Editorial Board member and the research group.

Supplementary information accompanies this paper at (https://www.maxapress.com/article/doi/10.48130/vns-0025-0004)

Dates

Received 11 February 2025; Revised 20 February 2025; Accepted 26 February 2025; Published online 27 March 2025

References

1. Hartnett ME, Penn JS. 2012. Mechanisms and management of retinopathy of prematurity. *New England Journal of Medicine* 367:2515–26
2. Hellström A, Smith LE, Dammann O. 2013. Retinopathy of prematurity. *The lancet* 382:1445–57
3. Schaffer DB, Palmer EA, Plotsky DF, Metz HS, Flynn JT, et al. 1993. Prognostic factors in the natural course of retinopathy of prematurity. *Ophthalmology* 100:230–37
4. Yu H, Yuan L, Zou Y, Peng L, Wang Y, et al. 2014. Serum concentrations of cytokines in infants with retinopathy of prematurity. *APMIS* 122:818–23
5. Bancalari A, Schade R. 2022. Update in the Treatment of Retinopathy of Prematurity. *American Journal of Perinatology* 39:22–30
6. Hartnett ME, Stahl A. 2023. Laser versus Anti-VEGF: A Paradigm Shift for Treatment-Warranted Retinopathy of Prematurity. *Ophthalmology and Therapy* 12:2241–52
7. Houston SK, Wykoff CC, Berrocal AM, Hess DJ, Murray TG. 2013. Laser treatment for retinopathy of prematurity. *Lasers in Medical Science* 28:683–92
8. Takano F, Ueda K, Yamada-Nakanishi Y, Nakamura M. 2024. Comparison of Single-Treatment Efficacy of Bevacizumab and Ranibizumab for Retinopathy of Prematurity. *Children* 11:927
9. Hartnett ME. 2020. Retinopathy of Prematurity: Evolving Treatment With Anti-Vascular Endothelial Growth Factor. *Am J Ophthalmol* 218:208–13
10. Tran KD, Cernichiaro-Espinosa LA, Berrocal AM. 2018. Management of Retinopathy of Prematurity-Use of Anti-VEGF Therapy. *Asia-Pacific Journal of Ophthalmology* 7:56–62
11. Mintz-Hittner HA, Kennedy KA, Chuang AZ. 2011. Efficacy of intravitreal bevacizumab for stage 3+ retinopathy of prematurity. *New England Journal of Medicine* 364:603–15
12. Martínez-Castellanos MA, Ortiz-Ramirez GY. 2021. Surgery for stage 5 retinopathy of prematurity. *Current Opinion in Ophthalmology* 32:482–88
13. Papageorgiou E, Riri K, Kardaras D, Grivea I, Mataftsi A, et al. 2022. Scleral buckling surgery for stage 4A and 4B retinopathy of prematurity in critically ill neonates. *International Ophthalmology* 42:1093–100
14. Wu Q, Hu Y, Mo Z, Wu R, Zhang X, et al. 2022. Development and Validation of a Deep Learning Model to Predict the Occurrence and Severity of Retinopathy of Prematurity. *JAMA Network Open* 5:e2217447
15. Connor KM, Krah NM, Dennison RJ, Aderman CM, Chen J, et al. 2009. Quantification of oxygen-induced retinopathy in the mouse: a model of vessel loss, vessel regrowth and pathological angiogenesis. *Nature protocols* 4:1565–73
16. Grossniklaus HE, Kang SJ, Berglin L. 2010. Animal models of choroidal and retinal neovascularization. *Progress in Retinal and Eye Research* 29:500–19
17. Selvam S, Kumar T, Fruttiger M. 2018. Retinal vasculature development in health and disease. *Progress in Retinal and Eye Research* 63:1–19
18. Melecchi A, Canovai A, Amato R, Dal Monte M, Filippi L, et al. 2024. Agonism of β3-Adrenoceptors Inhibits Pathological Retinal Angiogenesis in the Model of Oxygen-Induced Retinopathy. *Investigative Ophthalmology & Visual Science* 65:34
19. Bisen S, Verma SK, Mukhopadhyay CS, Singh NK. 2024. A neutrophil elastase-generated mature form of IL-33 is a potent regulator of endothelial cell activation and proliferative retinopathy. *Experimental & Molecular Medicine* 56:1703–16
20. Elbedwehy AM, Wu J, Na HK, Baek A, Jung H, et al. 2024. ROS-responsive charge reversal mesoporous silica nanoparticles as promising drug delivery system for neovascular retinal diseases. *Journal of Controlled Release* 373:224–39
21. Hu J, Song X, He YQ, Freeman C, Parish CR, et al. 2012. Heparanase and vascular endothelial growth factor expression is increased in hypoxia-induced retinal neovascularization. *Investigative Ophthalmology & Visual Science* 53:6810–17
22. Alon T, Hemo I, Itin A, Pe'er J, Stone J, et al. 1995. Vascular endothelial growth factor acts as a survival factor for newly formed retinal vessels and has implications for retinopathy of prematurity. *Nature Medicine* 1:1024–28
23. Yamada H, Yamada E, Hackett SF, Ozaki H, Okamoto N, et al. 1999. Hyperoxia causes decreased expression of vascular endothelial growth factor and endothelial cell apoptosis in adult retina. *Journal of cellular physiology* 179:149–56
24. Gu X, El-Remessy AB, Brooks SE, Al-Shabrawey M, Tsai NT, et al. 2003. Hyperoxia induces retinal vascular endothelial cell apoptosis through formation of peroxynitrite. *American Journal of Physiology-Cell Physiology* 285:C546–C54
25. Suzumura A, Terao R, Kaneko H. 2020. Protective effects and molecular signaling of n-3 fatty acids on oxidative stress and inflammation in retinal diseases. *Antioxidants* 9:920
26. Ninchoji T, Love DT, Smith RO, Hedlund M, Vestweber D, et al. 2021. eNOS-induced vascular barrier disruption in retinopathy by c-Src activation and tyrosine phosphorylation of VE-cadherin. *eLife* 10:e64944
27. Smith TL, Oubaha M, Cagnone G, Boscher C, Kim JS, et al. 2022. eNOS controls angiogenic sprouting and retinal neovascularization through the regulation of endothelial cell polarity. *Cellular and Molecular Life Sciences* 79:37
28. Zhu G, Lin Y, Liu H, Jiang D, Singh S, et al. 2018. Dll4-Notch1 signaling but not VEGF-A is essential for hyperoxia induced vessel regression in retina. *Biochemical and Biophysical Research Communications* 507:400–6
29. Wang L, Shi P, Xu Z, Li J, Xie Y, et al. 2014. Up-regulation of VEGF by retinoic acid during hyperoxia prevents retinal neovascularization and retinopathy. *Investigative Ophthalmology & Visual Science* 55:4276–87
30. Ozaki NK, Beharry KD, Nishihara KC, Akmal Y, Ang JG, et al. 2002. Regulation of retinal vascular endothelial growth factor and receptors in rabbits exposed to hyperoxia. *Investigative Ophthalmology & Visual Science* 43:1546–57
31. Stellmach V, Crawford SE, Zhou W, Bouck N. 2001. Prevention of ischemia-induced retinopathy by the natural ocular antiangiogenic agent pigment epithelium-derived factor. *Proceedings of the National Academy of Sciences of the United States of America* 98:2593–97
32. Huang Q, Wang S, Sorenson CM, Sheibani N. 2008. PEDF-deficient mice exhibit an enhanced rate of retinal vascular expansion and are more sensitive to hyperoxia-mediated vessel obliteration. *Experimental Eye Research* 87:226–41
33. Calzi SL, Shaw LC, Moldovan L, Shelley WC, Qi X, et al. 2019. Progenitor cell combination normalizes retinal vascular development in the oxygen-induced retinopathy (OIR) model. *JCI Insight* 4:e129224
34. Wang Yn, Gao S, Gao S, Li N, Xie B, et al. 2021. Blocking the interaction between interleukin-17A and endoplasmic reticulum stress in macrophage attenuates retinal neovascularization in oxygen-induced retinopathy. *Cell & Bioscience* 11:82
35. Liu CQ, Liu XY, Ouyang PW, Liu Q, Huang XM, et al. 2023. Ferrostatin-1 attenuates pathological angiogenesis in oxygen-induced retinopathy via inhibition of ferroptosis. *Experimental eye research* 226:109347
36. Santos AM, Calvente R, Tassi M, Carrasco MC, Martín-Oliva D, et al. 2008. Embryonic and postnatal development of microglial cells in the mouse retina. *Journal of Comparative Neurology* 506:224–39
37. Li F, Jiang D, Samuel MA. 2019. Microglia in the developing retina. *Neural Development* 14:12
38. Han X, Chen X, Chen S, Luo Q, Liu X, et al. 2020. Tetramethylpyrazine attenuates endotoxin-induced retinal inflammation by inhibiting

microglial activation via the TLR4/NF-κB signalling pathway. *Biomedicine & Pharmacotherapy* 128:110273
39. Checchin D, Sennlaub F, Levavasseur E, Leduc M, Chemtob S. 2006. Potential role of microglia in retinal blood vessel formation. *Investigative Ophthalmology & Visual Science* 47:3595–602
40. Hu A, Schmidt MHH, Heinig N. 2024. Microglia in retinal angiogenesis and diabetic retinopathy. *Angiogenesis* 27:311–31
41. Xu W, Hu Z, Lv Y, Dou G, Zhang Z, et al. 2018. Microglial density determines the appearance of pathological neovascular tufts in oxygen-induced retinopathy. *Cell and Tissue Research* 374:25–38
42. Zhao C, Liu Y, Meng J, Wang X, Liu X, et al. 2022. LGALS3BP in microglia promotes retinal angiogenesis through PI3K/AKT pathway during hypoxia. *Investigative Ophthalmology & Visual Science* 63:25
43. He C, Liu Y, Huang Z, Yang Z, Zhou T, et al. 2021. A specific RIP3^{+} subpopulation of microglia promotes retinopathy through a hypoxia-triggered necroptotic mechanism. *Proceedings of the National Academy of Sciences of the United States of America* 118:e2023290118
44. Li J, Yu S, Lu X, Cui K, Tang X, et al. 2021. The phase changes of M1/M2 phenotype of microglia/macrophage following oxygen-induced retinopathy in mice. *Inflammation Research* 70:183–92
45. Usui-Ouchi A, Eade K, Giles S, Ideguchi Y, Ouchi Y, et al. 2022. Deletion of Tgfβ signal in activated microglia prolongs hypoxia-induced retinal neovascularization enhancing Igf1 expression and retinal leukostasis. *Glia* 70:1762–76
46. Luo Q, Jiang Z, Jiang J, Wan L, Li Y, et al. 2023. Tsp-1^{+} microglia attenuate retinal neovascularization by maintaining the expression of Smad3 in endothelial cells through exosomes with decreased miR-27a-5p. *Theranostics* 13:3689–706
47. Chen X, Wang X, Cui Z, Luo Q, Jiang Z, et al. 2023. M1 microglia-derived exosomes promote activation of resting microglia and amplifies proangiogenic effects through Irf1/miR-155-5p/Socs1 axis in the retina. *International Journal of Biological Sciences* 19:1791–812
48. Green KN, Crapser JD, Hohsfield LA. 2020. To kill a microglia: a case for CSF1R inhibitors. *Trends in Immunology* 41:771–84
49. Spangenberg E, Severson PL, Hohsfield LA, Crapser J, Zhang J, et al. 2019. Sustained microglial depletion with CSF1R inhibitor impairs parenchymal plaque development in an Alzheimer's disease model. *Nature Communications* 10:3758
50. Liu YJ, Spangenberg EE, Tang B, Holmes TC, Green KN, et al. 2021. Microglia elimination increases neural circuit connectivity and activity in adult mouse cortex. *Journal of Neuroscience* 41:1274–87
51. Feng X, Valdearcos M, Uchida Y, Lutrin D, Maze M, et al. 2017. Microglia mediate postoperative hippocampal inflammation and cognitive decline in mice. *JCI Insight* 2:e91229
52. Church KA, Rodriguez D, Mendiola AS, Vanegas D, Gutierrez IL, et al. 2023. Pharmacological depletion of microglia alleviates neuronal and vascular damage in the diabetic CX3CR1-WT retina but not in CX3CR1-KO or hCX3CR1$^{I249/M280}$-expressing retina. *Frontiers in Immunology* 14:1130735
53. Zhou Z, Jing Y, Niu Y, Chang T, Sun J, et al. 2022. Distinguished functions of microglia in the two stages of oxygen-induced retinopathy: a novel target in the treatment of ischemic retinopathy. *Life* 12:1676
54. Schindelin J, Arganda-Carreras I, Frise E, Kaynig V, Longair M, et al. 2012. Fiji: an open-source platform for biological-image analysis. *Nature Methods* 9:676–82
55. Zudaire E, Gambardella L, Kurcz C, Vermeren S. 2011. A computational tool for quantitative analysis of vascular networks. *PLOS ONE* 6:e27385
56. Young KF, Gardner R, Sariana V, Whitman SA, Bartlett MJ, et al. 2021. Can quantifying morphology and TMEM119 expression distinguish between microglia and infiltrating macrophages after ischemic stroke and reperfusion in male and female mice? *Journal of Neuroinflammation* 18:58
57. Nugent AA, Lin K, van Lengerich B, Lianoglou S, Przybyla L, et al. 2020. TREM2 regulates microglial cholesterol metabolism upon chronic phagocytic challenge. *Neuron* 105:837–854.e9
58. Krasemann S, Madore C, Cialic R, Baufeld C, Calcagno N, et al. 2017. The TREM2-APOE pathway drives the transcriptional phenotype of dysfunctional microglia in neurodegenerative diseases. *Immunity* 47:566–581.e9
59. Grubman A, Choo XY, Chew G, Ouyang JF, Sun G, et al. 2021. Transcriptional signature in microglia associated with Aβ plaque phagocytosis. *Nature Communications* 12:3015
60. Sun N, Victor MB, Park YP, Xiong X, Scannail AN, et al. 2023. Human microglial state dynamics in Alzheimer's disease progression. *Cell* 186:4386–4403.e29
61. Dejanovic B, Wu T, Tsai MC, Graykowski D, Gandham VD, et al. 2022. Complement C1q-dependent excitatory and inhibitory synapse elimination by astrocytes and microglia in Alzheimer's disease mouse models. *Nature Aging* 2:837–50
62. Kokkosis AG, Madeira MM, Hage Z, Valais K, Koliatsis D, et al. 2024. Chronic psychosocial stress triggers microglial-/macrophage-induced inflammatory responses leading to neuronal dysfunction and depressive-related behavior. *Glia* 72:111–32
63. Thi Lai T, Kim YE, Nguyen LTN, Thi Nguyen T, Kwak IH, et al. 2024. Microglial inhibition alleviates alpha-synuclein propagation and neurodegeneration in Parkinson's disease mouse model. *NPJ Parkinson's Disease* 10:32
64. Montilla A, Zabala A, Er-Lukowiak M, Rissiek B, Magnus T, et al. 2023. Microglia and meningeal macrophages depletion delays the onset of experimental autoimmune encephalomyelitis. *Cell Death & Disease* 14:16
65. Mou Q, Yao K, Ye M, Zhao B, Hu Y, et al. 2021. Modulation of sirt1-mTORC1 pathway in microglia attenuates retinal ganglion cell loss after optic nerve injury. *Journal of Inflammation Research* 14:6857–69
66. Church KA, Rodriguez D, Vanegas D, Gutierrez IL, Cardona SM, et al. 2022. Models of microglia depletion and replenishment elicit protective effects to alleviate vascular and neuronal damage in the diabetic murine retina. *Journal of Neuroinflammation* 19:300
67. Cheng Y, Javonillo DI, Pachow C, Scarfone VM, Fernandez K, et al. 2023. Ablation of microglia following infection of the central nervous system with a neurotropic murine coronavirus infection leads to increased demyelination and impaired remyelination. *Journal of Neuroimmunology* 381:578133
68. Brown FN, Iwasawa E, Shula C, Fugate EM, Lindquist DM, et al. 2023. Early postnatal microglial ablation in the *Ccdc39* mouse model reveals adverse effects on brain development and in neonatal hydrocephalus. *Fluids and Barriers of the CNS* 20:42
69. von Arx AS, Dawson K, Lin HY, Mattei D, Notter T, et al. 2023. Prefrontal microglia deficiency during adolescence disrupts adult cognitive functions and synaptic structures: a follow-up study in female mice. *Brain, Behavior, and Immunity* 111:230–46
70. Sariol A, Mackin S, Allred MG, Ma C, Zhou Y, et al. 2020. Microglia depletion exacerbates demyelination and impairs remyelination in a neurotropic coronavirus infection. *Proceedings of the National Academy of Sciences of the United States of America* 117:24464–74
71. Ye L, Shu S, Jia J, Sun M, Xu S, et al. 2023. Absent in melanoma 2 mediates aging-related cognitive dysfunction by acting on complement-dependent microglial phagocytosis. *Aging Cell* 22:e13860
72. Wilton DK, Mastro K, Heller MD, Gergits FW, Willing CR, et al. 2023. Microglia and complement mediate early corticostriatal synapse loss and cognitive dysfunction in Huntington's disease. *Nature Medicine* 29:2866–84
73. Zhou ZY, Chang TF, Lin ZB, Jing YT, Wen LS, et al. 2023. Microglial Galectin3 enhances endothelial metabolism and promotes pathological angiogenesis via Notch inhibition by competitively binding to Jag1. *Cell Death & Disease* 14:380
74. Gedam M, Comerota MM, Propson NE, Chen T, Jin F, et al. 2023. Complement C3aR depletion reverses HIF-1α-induced metabolic impairment and enhances microglial response to Aβ pathology. *Journal of Clinical Investigation* 133:e167501
75. Tabor SJ, Yuda K, Deck J, Gnanaguru G, Connor KM. 2023. Retinal injury activates complement expression in Müller cells leading to neuroinflammation and photoreceptor cell death. *Cells* 12:1754